

Heat Transfer Engineering

ISSN: 0145-7632 (Print) 1521-0537 (Online) Journal homepage: www.tandfonline.com/journals/uhte20

Numerical Investigation on Pool Boiling Heat Transfer of Silica and Alumina Nanofluids

Sudhir Kumar Singh, Deepak Sharma & Akshay Kumar Singh

To cite this article: Sudhir Kumar Singh, Deepak Sharma & Akshay Kumar Singh (2024) Numerical Investigation on Pool Boiling Heat Transfer of Silica and Alumina Nanofluids, Heat Transfer Engineering, 45:9, 728-747, DOI: 10.1080/01457632.2023.2220471

To link to this article: https://doi.org/10.1080/01457632.2023.2220471

Published online: 12 Jun 2023.

Submit your article to this journal

Article views: 361

View related articles

View Crossmark data

Citing articles: 10 View citing articles

Full Terms & Conditions of access and use can be found at
https://www.tandfonline.com/action/journalInformation?journalCode=uhte20

HEAT TRANSFER ENGINEERING
2024, VOL. 45, NO. 9, 728–747
https://doi.org/10.1080/01457632.2023.2220471

Taylor & Francis
Taylor & Francis Group

Check for updates

Numerical Investigation on Pool Boiling Heat Transfer of Silica and Alumina Nanofluids

Sudhir Kumar Singh, Deepak Sharma, and Akshay Kumar Singh

Department of Mechanical Engineering, National Institute of Technology Hamirpur, Hamirpur, India

ABSTRACT

Surface modification through pool boiling of nanofluid is an efficient technique in delaying critical heat flux and attaining high heat flux at lower wall superheat temperature. The method of involving phase interaction, bubble evolving and dynamics phenomenon, and distribution of vapor void fraction altogether is the motivation behind current topic. The present work will contribute to the recovery and reuse of the wastewater and incinerator heat, cooling of high heat flux generating micro-electronics chips, and cooling of fast breeder test reactors. In the present study, the nucleate pool boiling of SiO_2/water and Al_2O_3/water nanofluid are studied numerically and the effect of wall superheat temperature and heat flux on active nucleation site density, bubble departure diameter, and bubble waiting time are studied. The effect of various heater surface material and nanofluid concentration on wall superheat temperature and heat transfer coefficient are also investigated. A two-phase Eulerian approach, heat flux wall-partitioning model, and Rensselaer Polytechnic Institute boiling model are considered to simulate the current model. The pool boiling of nanofluids resulted in the formation of nano-porous layer on heater surface because of microlayer evaporation process that enhanced the heat transfer coefficient and reduced the wall superheat temperature.

Introduction

The application of nucleate pool boiling (NPB) for the enhancement of heat transfer processes such as cooling of fast breeder test reactor in which reactor core is placed inside the coolant, cooling of boilers tubes, and cooling of high heat flux generating micro-electronic equipment's [1] has emerged in the recent years. The heat dissipated from the microchip reaches up to 2000 kW/m^2 and in some circumstance, on-chip hot spot heat flux reaches as high as 15,000 kW/m^2 [2]. In nucleate region of pool boiling curve, high heat flux can be attained at a lower temperature difference and maximum heat transfer rate can be achieved. Due to this reason, all high heat flux generating equipment's are operated under NPB region [3]. Therefore, cooling of such systems under the NPB region has become one of the most predominant methods. However, the thermal performance of the devices is restricted by the critical heat flux (CHF) which is also called as boiling crisis and causes a localized overheating at the heater wall which results in decrement in heat transfer rate [4]. Several methods are used by the researchers in delaying the CHF, surface modification through pool boiling of nanofluid is one of the most efficient techniques used by researchers in recent years. The formation of micro/nano porous surface through nanoparticle deposition on heater surface enhances the wettability, porosity, nucleation site density, bubble departure diameter, and bubble releasing frequency [5]. Phase change occurrence from liquid to vapor establishes the boiling an efficient process for larger heat flux dissipation. Multi-phase heat transfer method employs a greater latent heat of vaporization, permitting it for enhanced heat transfer at a relatively lower temperature difference. Furthermore, the NPB heat transfer are required to be enhanced for greater efficiency of the system used for various applications.

Numerous studies on pool boiling have been conducted for thermal analysis. Aminfar et al. [6] numerically studied the multi-phase mixture model to analyze the boiling phenomenon of SiO_2/water nanofluid. Two-phase simulation model showed more accurate results than three-phase mixture model. Yeom et al. [7] studied the bubble behavior of Ti and

CONTACT Assistant Professor Deepak Sharma dsharma@nith.ac.in Mechanical Engineering Department, National Institute of Technology Hamirpur, Hamirpur 177005, H.P., India.

© 2023 Taylor & Francis Group, LLC

NOMENCLATURE

A_{conv}	fractions of boiling surface area associated to convection
A_{evap}	fractions of boiling surface area associated to evaporation
A_{quen}	fractions of the boiling surface area associated to quenching
a_{if}	interfacial area concentration (per meter)
Al	aluminum
Al_2O_3	aluminum oxide
CHF	critical heat flux, W/m^2
Cu	copper
C_D	drag coefficient
$C_{D,\ dis}$	distorted drag coefficient
$C_{D,\ vis}$	viscous drag coefficient
C_L	shear lift coefficient
C_p	specific heat, kJ/(kg K)
C_{TD}	turbulence dispersive constant in Eq. (10)
C_v	mass fraction of vapor phase
C_{w1}, C_{w2}	heater wall lubrication constant in Eq. (9)
C_{wf}	coefficient in Eq. (44) which depends on heater surface–fluid
C_{wt}	bubble waiting time coefficient
D_b	bubble diameter, m
D_d	bubble departure diameter, m
E_T	turbulent kinetic energy, J
f_b	bubble releasing frequency, Hz
f_i	scalar quantity associated with the detached bubble density
F_{fv}	impact of interfacial force on liquid by vapor phase, N
F_{vf}	impact of interfacial force from on vapor by liquid phase, N
F_{fv}^{drag}	drag force, N
F_{fv}^{lub}	wall lubrication force, N
F_{fv}^{lift}	Lift force, N
F_{fv}^{TD}	turbulence dispersive force, N
g	gravitational acceleration, m/s^2
HTC	heat transfer coefficient, kW/(m^2 K)
h	interfacial heat transfer coefficient, kW/(m^2 K)
h_T	heat transfer coefficient due to turbulency, kW/(m^2 K)
h_{fg}	latent heat of vaporization, kJ/kg
H	enthalpy, kJ/kg
k	thermal conductivity, kW/(m K)
$\dot{m}_{fv}$	interfacial mass transfer due to condensation, kg/(m^3 s)
$\dot{m}_{vf}$	interfacial mass transfer due to evaporation, kg/(m^3 s)
n	Index in Eq. (33)
$\hat{n}$	normal unit vector for the inter-phase
N_a	active nucleation sites density, sites/cm^2
Nu	Nusselt number
NPB	nucleate pool boiling
P	pressure, N/m^2
Pr	Prandtl number
Pt	platinum
Q_e	heat transfer rate due to evaporation, W
q''	heat flux, W/m^2
q''_{conv}	heat flux due to free convection, W/m^2
q''_{evap}	heat flux due to evaporation, W/m^2
q''_{quen}	heat flux due to free quenching, W/m^2
Re	Reynolds number
RPI	Rensselaer Polytechnic Institute
S_i	source terms because of bubble merging and separation, kg/(m^3 s)
SiO_2	silicon oxide
t	time, s
T	temperature, K
ΔT_{sup}	wall superheat temperature ($T_w - T_{sat}$), K
t_{bw}	bubble waiting time, s
TiO_2	titanium oxide
$\vec{u}_f$, $\vec{u}_v$	velocity of liquid and vapor phase respectively, m/s
$\vec{u}_{f,i}$, $\vec{u}_{f,j}$	velocity of liquid phase along x_i and x_j direction respectively, m/s
$\vec{u}_{v,i}$, $\vec{u}_{v,j}$	velocity of vapor phase along x_i and x_j direction, m/s
$\vec{u}_{vf}$	relative velocity of vapor phase to that of liquid phase, m/s
$\vec{u}_{dr}$	drift velocity, m/s
x_i, x_j	Cartesian coordinate along x and y direction respectively, m
y_w	vertical distance from heater wall, m

Greek symbols

α	void fraction
μ	dynamic viscosity, N·s/m^2
ρ	density, kg/m^3
σ	surface tension, N/m
φ	volume concentration, %
θ	contact angle of fluid on surface, degree

Subscripts

atm	atmospheric
bf	base fluid
nf	nanofluid
ONB	onset of nucleate boiling
p	nanoparticle
f	liquid phase
mix	mixture
sat	saturation
sup	superheat
v	vapor phase
w	heater wall

TiO_2 coated on zirconium wire for NPB heat transfer. Electrophoretic deposition method was used to deposit 60–80 mm thick TiO_2 nanomaterial on 0.6 mm zirconium wire. CHF enhanced by 27% and 65% for titanium and TiO_2 respectively than plain wire. Nucleation site density of titanium and TiO_2-coated surface was 47 and 45% lower than plain wire at 300 kw/m^2 heat flux. Kiyomura et al. [8] examined the influence of nanomaterial deposition and surface roughness on wettability and heat transfer coefficient (HTC). The nanostructured surface was developed by maghemite nanomaterial coating, which was achieved by NPB process of ferric oxide/water nanofluid (0.03–0.3 g/L mass concentration). The experiments were conducted on Cu heater surface, de-ionized water as pool boiling fluid, and saturated condition. The maximum HTC was observed for the smooth surface with decreased mass concentration modified surface.

Nazari and Saedodin [9] developed the Al_2O_3 coating on Al heater surface using anodic-oxidation technique considering deionized water as working fluid. Surface modification on test heater surface enhanced the CHF and HTC. The enhancement was because of improved surface wettability and nucleation sites. An increase in pore size of modified surface resulted in wettability reduction. CHF and HTC enhanced by 70% and 28%, respectively.

Song et al. [10] utilized electrophoretic deposition method to develop nano-porous surface of alumina on stainless steel surface. SES36 was considered as working fluid. Alumina nanoparticle of 0.5–2 wt% concentration was dispersed in SES36 boiling fluid. HTC was enhanced by 77% at 90 kW/m^2 heat flux. An enhancement in HTC was mainly because of improved nucleation site density. Quan et al. [11] studied the wettability effect of SiO_2-deposited modified surface. Enhanced CHF with nanofluid having moderate hydrophilic nature nanoparticle while reduced HTC with strong hydrophilic nature nanoparticle was observed. This was mainly due to the rough and irregular nanoparticle coated layer for moderate case. Noh et al. [12] studied the boiling behavior of SiO_2 coated on microstructured surface. The influence of deflection point on HTC was investigated. The deflection was observed at greater heat flux and HTC of SiO_2 coated surface and plain heater surface of 3.27 and 4.67 kW/m^2 K, respectively. Ray and Bhaumik [13] studied pool boiling of R-134a on TiO_2 nanomaterial deposited surface. Electron beam evaporation technique was utilized to deposit the nanoparticle of thickness 100–300 nm on Cu heater surface. HTC enhanced by 88% for 300 nm coating thickness. Incipience wall superheat was decreased for greater coating thickness. Abadi and coworkers [14] performed simulation on pool boiling in vertically aligned circular tube. Rensselaer Polytechnic Institute (RPI) model and Eulerian approach was used to formulate the boiling phenomenon.

Gobinath et al. [15] numerically investigated the subcooled pool boiling of Al_2O_3/water nanofluid. Pressure-based implicit function and SIMPLE technique were used to discretize and solve the problem. Gupta et al. [16] performed simulation on boiling of nanofluid using transient Eulerian multiphase method. Simulation was performed on two-dimensional geometrical model. An increment in HTC was observed with rise in heat flux and volume concentration of nanofluid. For constant heat flux, HTC enhanced with increase in pressure. Wang et al. [17] numerically studied the NPB having different heater surface geometries. Heater surface having 36 hemispheres in various orientation are developed. The boiling chamber with modified heating surface showed enhanced heat transfer than bared heater surface. The boiling surface having downward facing hemispheres showed best configuration among all others. Pourfattah et al. [18] performed a simulation on Cupric oxide/water nanofluid boiling. A Eulerian–Eulerian approach and phase change process was used. The phase change position and bubble formation were influenced with change in volume concentration of nanofluid.

Akbari et al. [19] studied the saturated pool boiling of graphene nanofluid. At constant concentration, the thermal conductivity of functionalized graphene was greater than pure graphene. Kamel et al. [20] used Eulerian-multiphase model to perform the numerical simulation of SiO_2/water nanofluid boiling. The boiling curve behavior and phase interaction was investigated considering heat flux partitioning model. Çiftçi and Sözen [21] performed simulation on boiling of SiO_2/dichloromethane nanofluid and hexagonal boron nitride/dichloromethane nanofluid. The numerical simulation was performed for analyzing the evaporation-condensation phenomenon of nanofluid. Singh and Sharma [22] reviewed the effect of nanomaterial deposition through boiling process of nanofluid on pool boiling heat transfer performance. An improvement in CHF was obtained using micro–nanostructured surface. Fabrication of hydrophilic surface resulted in enhanced HTC. Zaboli et al. [23] performed simulation on pool boiling of SiO_2/water nanofluid and studied their bubble dynamic behavior. An increment in HTC of 50% was achieved at concentration of 0.1%.

Harikrishnan et al. [24] studied the influence of nanoparticle, their concentration, and surfactant on the surface tension of nanofluid using the pendant drop method. An increase in nanoparticle concentration resulted in an enhancement in surface tension in the absence of surfactant whereas a decrement in surface tension with increase in nanoparticle concentration was obtained with the combined nanoparticle and surfactant combination. Harikrishnan et al. [25] studied the combined effect of surfactant and nanoparticles on the wettability of nanofluids on different surfaces. The combined nanoparticle–surfactant colloidal showed wetting characteristics on all substrates. The combined nanoparticle–surfactant colloidal at all nanoparticle concentration showed wettability much lower as compared to that for the surfactant-alone case at the same surfactant concentration. Harikrishnan et al. [26] developed a mathematical model to predict

the surface tension and wettability of surfactant-capped nanoparticles. The proposed model was based on the governing role of mechanical, chemical, thermal and electrostatic equilibrium parameter involving the concept of interfacial adsorption–desorption behavior of nanosized particles due to the interactions and interfaces involvement at the nanoscale.

As stated earlier, a wide range of research has been performed to enhance the pool boiling heat transfer. There is no doubt that the surface modification and fluid properties influence the heat transfer performance. However, to the best knowledge of the authors, a numerical simulation on the pool boiling of Al_2O_3/water nanofluid having wide range of volume concentration is missing. Most of the simulation work is on the pool boiling of silica nanofluid with single or limited nanoparticle concentration. A detailed understanding of phase interaction mechanism, bubble evolution, and bubble dynamics behavior such as active nucleation site density, bubble departure diameter, bubble departure time, bubble waiting time, and distribution of vapor void fraction is still limited and there is a shortage of literature that considers the bubble dynamics phenomenon altogether. Due to the complexity in heat transfer mechanisms while modeling and simulation of pool boiling, various researchers have utilized an empirical correlation with distinct parameters, but very limited research were found on the importance of microlayer in bubble evolving process. For the effective application of NPB, a thorough understanding of basic physics of saturated pool boiling phenomenon and its associated heat transfer mechanism is essential. The numerical investigation of pool boiling of Al_2O_3/water nanofluid having concentration of 0.01–0.06 vol% involving phase interaction mechanism, bubble evolving process, bubble dynamics phenomenon, and distribution of vapor void fraction altogether is considered as the novelty of current study. The motivation of the present study is of great importance and will contribute to the recovery and reuse of the wastewater and incinerator heat, reduction in energy dissipation or cooling of high heat generating micro-electronic equipment, cooling of fast breeder test reactor in which reactor core is placed inside the coolant.

In present study, the pool boiling of SiO_2/water and Al_2O_3/water nanofluid having concentration of 0.01–0.06 vol% under saturated boiling condition are studied numerically using two-phase Eulerian approach and heat flux wall-partitioning model with an aim of generation of small nanoporous cavities and increased active nucleation sites. The effect of nanofluid concentration, heater surface material, and heat flux on wall superheat temperature and pool boiling heat transfer coefficient are investigated. A variation in nucleation site density, bubble departure diameter, and bubble waiting time with heat flux and superheat temperature are studied. A wide range of heat flux is considered to examine the influence of nanoparticle deposited heater surface on the thermal performance.

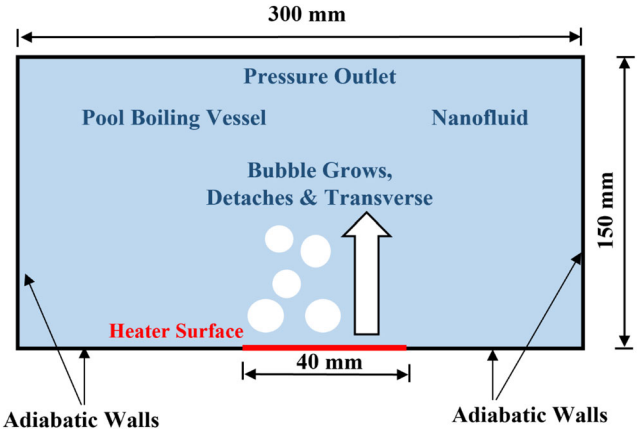

Figure 1. Two-dimensional representation of computational domain.

Description of computational domain

A two-dimensional computational domain for pool boiling of nanofluid can be seen in Figure 1. A pool boiling vessel of 300 mm × 150 mm dimension and copper heater surface of 40 mm length is considered. The pool boiling of nanofluid is simulated under saturated boiling and atmospheric pressure condition. A heat flux ranging from 100 to 600 kW/m^2 is provided to the heater surface and adiabatic condition are provided to the lateral wall of chamber. The pool boiling heat transfer characteristics and bubble dynamic behavior was modeled, simulated, and solved numerically using ANSYS FLUENT software. Other detailed parameters of the numerical simulation settings can be seen from Table 1.

Theoretical formulation

Assumption

Eulerian multiphase model (two-phase model) is considered for pool boiling of nanofluid. In this model, the liquid acts as a continuum phase and vapor behaves as a dispersive phase. The dilute aqueous nanofluids with low concentration (less than 0.1 vol%) are supposed to be favorable coolants for safety systems in fast breeder nuclear reactors (important

Table 1. Numerical simulation set-up conditions setting in ANSYS FLUENT software.

Set-up conditions	Parameters	Selected
General	Model	2-D Transient
	Solver type	Pressure based
	Velocity Formulation	Absolute
	Gravitational acceleration	Y axis, −9.71 m/s^2
Multiphase model	Model	Eulerian
	Number of Eulerian phases	Two
	Eulerian parameters	RPI Boiling Model
	Volume Fraction Parameters Formulation	Implicit
Phase	Primary phase	Liquid
	Secondary phase	Vapor
Phase interaction	Phase pair	Liquid-vapor
	Drag coefficient	Ishii-Zuber
	Lift coefficient	Tomiyama
	Wall lubrication	Antal et al.
	Turbulent dispersion	Lopez-de-Bertodano
	Turbulent interaction	Troshko-Hassan
	Surface tension (Water at 100 °C)	0.0589 N/m
Viscous model	Model	k-epsilon (2 eq.)
	Near-wall treatment	Enhanced wall treatment
Solution methods	Pressure-velocity coupling	Phase-coupled SIMPLE
	Gradient	Least squares cell based
	Pressure	PRESTO
	Turbulent kinetic energy	First-order upwind
	Turbulent dissipation rate	First-order upwind
	Momentum and energy	First-order upwind
	Volume fraction	Modified HRIC
	Transient formulation	First order implicit

application of pool boiling) because of their capability for improving the CHF with insignificant change in thermo-physical properties as related to that of base fluid [27]. A dilute nanofluid acts as hydrodynamically identical to its base fluid and theoretically can be considered as a single liquid regardless of the existence of two different phases which has permitted a development of thermofluidic dynamic models for nanofluids established on the Navier–Stokes equations. A single-phase computational model having base liquid-nanoparticle as a single-phase has an accuracy related to that of a two-phase model in which the liquid and the nanoparticle phase are considered independently on condition that the suspension properties are accurately formulated. Therefore, it is admissible to consider the Eulerian multiphase two-fluid model [27]. Apart from this, we have assumed an insignificant change in thermo-physical properties of vapor phase with stabled nanoparticles. Furthermore, it is also presumed that the energy transfer from the heater surface (boiling surface) to the working fluid is completely utilized for the vapor formation.

Governing equations

Continuity, momentum, and energy equations

A two-phase mixture model is opted for the current numerical simulation in which nanofluid behaves as a continuum phase and vapor behaves as dispersive phase [28]. The mixture model is the simplest two-phase mixture model, which are utilized to model the two-phase flows where both the phases propagate with different velocities like in the case of pool boiling. In the mixture model, a strong connection between both the phases occurs, which helps to model the homogeneous multiphase flow with strong bonding where both the phases propagate at the equal speed. The set-up conditions for the present model can be seen in Table 1.

In the current numerical simulation of two-phase flows, the mass, momentum, and energy equation are solved separately for individual phase considering Eulerian–Eulerian method [29].

Continuity equation for continuum phase (liquid)

$$\frac{\partial(\rho_f \alpha_f)}{\partial t} + \nabla.\left(\rho_f.\alpha_f.\vec{u}_f\right) = \dot{m}_{fv} \tag{1}$$

Continuity equation for dispersive phase (vapor)

$$\frac{\partial(\rho_v \alpha_v f_i)}{\partial t} + \nabla.\left(\rho_v.\alpha_v.\vec{u}_v\right) = S_i - f_i.\dot{m}_{fv} \tag{2}$$

Momentum equation for liquid phase

$$\begin{aligned}\frac{\partial\left(\rho_f \alpha_f \vec{u}_{f,i}\right)}{\partial t} &+ \nabla.\left(\rho_f.\alpha_f.\vec{u}_{f,i}.\vec{u}_{f,j}\right) \\ &= -\alpha_f.\nabla P + \rho_f.\alpha_f.g + \nabla\left[\alpha_f.\mu_f^e\left(\nabla \vec{u}_f + \left(\vec{u}_f\right)^T\right)\right] \\ &+ \left(\dot{m}_{fv}\vec{u}_v - \dot{m}_{vf}\vec{u}_f\right) + F_{fv}\end{aligned} \tag{3}$$

Momentum equation for vapor phase

$$\begin{aligned}\frac{\partial\left(\rho_v \alpha_v \vec{u}_v\right)}{\partial t} &+ \nabla.\left(\rho_v.\alpha_v.\vec{u}_{v,i}\vec{u}_{v,j}\right) \\ &= -\alpha_v.\nabla P + \rho_v.\alpha_v.g + \nabla\left[\alpha_v.\mu_v^e\left(\nabla \vec{u}_v + \left(\nabla \vec{u}_v\right)^T\right)\right] \\ &+ \left(\dot{m}_{vf}\vec{u}_f - \dot{m}_{fv}\vec{u}_v\right) + F_{vf}\end{aligned} \tag{4}$$

Energy equation for liquid phase

$$\begin{aligned}\frac{\partial(\rho_f \alpha_f H_f)}{\partial t} &+ \nabla.\left(\rho_f.\alpha_f.\vec{u}_f.H_f\right) \\ &= \nabla\left[\alpha_f.k_f^e(\nabla T_f)\right] + \left(\dot{m}_{vf}H_f - \dot{m}_{fv}H_v\right)\end{aligned} \tag{5}$$

Energy equation for vapor phase

$$\begin{aligned}\frac{\partial(\rho_v \alpha_v H_v)}{\partial t} &+ \nabla.\left(\rho_v.\alpha_v.\vec{u}_v.H_v\right) \\ &= \nabla\left[\alpha_v.k_v^e(\nabla T_v)\right] + \left(\dot{m}_{fv}H_v - \dot{m}_{vf}H_f\right)\end{aligned} \tag{6}$$

where the subscript f and v indicate the phase, f corresponds to the liquid phase and v denotes the vapor phase.

Drag, lift, wall lubrication, and turbulent dispersion force for phase interaction

Heat and mass transfer are introduced to solve the governing equations expressing the inter-phase interaction that are associated to the interfacial momentum. The two-equations κ-ε model are considered, because of chaotic behavior of bubbles and dynamic behavior associated with them [30]. Drag and lift force along with turbulent dispersion force are originated due to the liquid–vapor phase interaction. The interfacial force (F_{fv}) in Eq. (3) existing in the liquid phase, consist of the drag force (F_{fv}^{drag}), lift force (F_{fv}^{lift}), wall lubrication force (F_{fv}^{lub}) and turbulence dispersive force (F_{fv}^{TD}) [29]. For the vapor phase in Eq. (4), $F_{vf} = -F_{fv}$. The drag force because of interfacial momentum transfer is expressed by [29]:

$$F_{fv}^{drag} = \frac{1}{8}\ C_D.a_{if}.\rho_f\left|\vec{u}_v - \vec{u}_f\right|\left(\vec{u}_v - \vec{u}_f\right) \tag{7}$$

The drag coefficient (C_D) in Eq. (7) has been correlated for various Re and individual vapor bubbles based on Ishii and Zuber [31]. The lift force because of interfacial momentum transfer is expressed by [29]:

$$F_{fv}^{lift} = C_L.\rho_f.\alpha_v\left(\vec{u}_v - \vec{u}_f\right) \times \left(\nabla\ \times \vec{u}_f\right) \tag{8}$$

where C_L in Eq. (8) is considered equal to 0.01 [32]. The wall lubrication force is perpendicular to the heater surface, and its effects neutralizes with vertical distance from the heater surface, is given by [29]:

$$F_{fv}^{lub} = -\ \frac{\rho_v.\alpha_v\left(\vec{u}_v - \vec{u}_f\right)}{D_b}\max\left(0,\ C_{w1} + C_{w2}\frac{D_b}{y_w}\right)\vec{n} \tag{9}$$

where, C_{w1} and C_{w2} are the heater wall lubrication constant and are considered equal to –0.01 and 0.05 respectively [33].

The chaotic dispersion force behaves as a turbulence diffusion in the dispersive flow. The turbulence dispersion forces (F_{fv}^{TD}), which is responsible for the inter-phase turbulence momentum transfer is given by [34]:

$$F_{fv}^{TD} = -\rho_f.E_{T,f}.C_{TD}.\nabla\alpha_v \tag{10}$$

where, C_{TD} is turbulence dispersive constant which is user-changeable constant and recommended value is 0.1 according to Cheung et al. [29].

The coefficient of drag (C_D) in Eq. (7) can be obtained by finding the minimum of viscous drag coefficient and distorted drag coefficient [33]

$$C_D = \min\left(C_{D,vis},\ C_{D,dis}\right) \tag{11}$$

The viscous drag coefficient ($C_{D,\ vis}$) and distorted drag coefficient ($C_{D,\ dis}$) in Eq. (11) are expressed by [20]:

$$C_{D,\ vis} = \frac{24}{Re}\ (1 + 0.15\ Re^{0.75}) \tag{12}$$

$$C_{D,\ dis} = \frac{2}{3}\ \frac{D_b}{\sqrt{\frac{\sigma}{g(\rho_f - \rho_v)}}} \tag{13}$$

The Reynolds number in Eq. (12) can be obtained by [20]:

$$Re = \frac{\rho_f\left|\vec{u}_v - \vec{u}_f\right|D_b}{\mu_f} \tag{14}$$

The interfacial mass transfer due to condensation and evaporation

The interfacial mass transfer due to condensation ($\dot{m}_{fv}$) and due to evaporation ($\dot{m}_{vf}$) in Eqs. (1)–(4) is expressed by [35]:

$$\dot{m}_{fv} = \frac{h.a_{if}.T_{sat}}{h_{fg}} \tag{15}$$

$$\dot{m}_{vf} = \frac{Q_e}{h_{fg}} \tag{16}$$

The non-thermal equilibrium around the inter-phase might results in accumulation of heat during heat interaction between liquid and vapor phase. The HTC between inter-phase interaction is obtained using Ranz [36] model. The interfacial heat transfer coefficient (h) in Eq. (15) are expressed by [35]:

$$h = \frac{k_f}{D_b}Nu_v \tag{17}$$

$$Nu_v = 2 + 0.6Pr_f^{0.333}Re_v^{0.5} \tag{18}$$

$$Pr_f = \frac{C_{p,f}.\mu_f}{k_f} \tag{19}$$

Volume fraction equation

The volume fraction can be obtained from continuity equation for vapor phase and is expressed as [6]:

$$\frac{\partial(\rho_v\alpha_v)}{\partial t} + \nabla.\left(\rho_v.\alpha_v.\vec{u}_{v,i}\right) = -\nabla.\left(\rho_v.\alpha_v.\vec{u}_{dr,v}\right) + \dot{m}_{fv} \tag{20}$$

$$\dot{m}_{fv} = \pm k_f\frac{\nabla T_f}{h_{fg}}\ \hat{n} \tag{21}$$

The negative and positive sign is considered for the liquid and vapor phase, respectively. The drift velocity of vapor phase ($\vec{u}_{dr,v}$) in Eq. (20) is given by [6]:

$$\vec{u}_{dr,v} = \vec{u}_{vf} - \sum_1^n C_v.\vec{u}_v \tag{22}$$

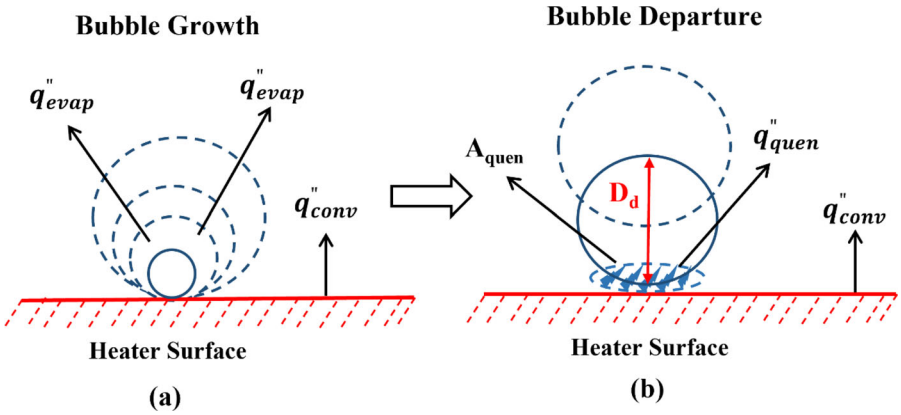

Figure 2. A schematic of heat flux wall partitioned model.

The relative velocity of vapor phase to that of liquid phase $(\vec{u}_{vf})$ and mass fraction of vapor phase (C_v) is expressed by [6]:

$$\vec{u}_{vf} = \vec{u}_v - \vec{u}_f \tag{23}$$

$$C_v = \frac{\rho_v.\alpha_v}{\rho_{mix}} \tag{24}$$

Heat flux wall partitioning method

Kurul and Podowski [37] established the well-known RPI model for pool boiling mechanisms of fluid. In this classical model, the entire supplied heat flux to the heater wall is controlled by three mechanisms. First, heat flux due to the free convection (q''_{conv}) which is the heat transferred from the nucleated bubbles to the bulk fluid. Second, the heat flux due to evaporation (q''_{evap}) which is defined as the quantity of heat which is associated to the evaporated fluid for the formation of bubble. Third, the heat flux due to quenching (q''_{quen}) which is the amount of heat associated with the disturbed fluid layer by the departed bubble from the heater wall. In other words, quenching heat flux is the phenomenon of transient conductive heat transfer for the liquid compensation of the wall domain after the separation of bubble. In simple words, heat flux due to quenching is the energy absorbed after bubble separation [32]. Figure 2 shows the schematic demonstration of mechanism involved in heat flux wall partitioned model.

The heat flux wall partitioning is expressed by [38].

$$q''_{Total} = q''_{conv} + q''_{evap} + q''_{quen} \tag{25}$$

$$q''_{conv} = \left[1 - \frac{\pi}{4A_{conv}} \sum_{n=1}^{N_a} \left(D^2_{d,n}\right)\right] h_T(T_w - T_{sat}) \tag{26}$$

$$q''_{evap} = \frac{\pi}{6A_{evap}} \rho_v.h_{fg}. \sum_{n=1}^{N_a} \left(D^3_{d,n}.f_{b,n}\right) \tag{27}$$

$$q''_{quen} = N_a \left[\frac{2\pi k_f (T_w - T_{sat})}{A_{quen}\sqrt{\pi\alpha_f}} \left(D^2_b.f_b\sqrt{t_{bw}}\right)\right] \tag{28}$$

Since no external movement of liquid in pool boiling, therefore turbulence heat transfer coefficient (h_T) can be neglected during calculation. The fractions of the boiling surface area associated to quenching (A_{quen}) can be seen in Figure 2.

Nucleation site density

The active nucleation site density is the function of alignment of cavities on the heater wall, heater wall material, working fluid properties, and hydrophilic or hydrophobic nature of wettability. As earlier mentioned, active nucleation site density performs a significant contribution for the assessment of the heat flux wall-partitioning model. The modified heater surface with nanoparticles deposition during pool boiling of nanofluid enhance the nucleation site density, bubble departure diameter, porosity, bubble release frequency, etc. Therefore, an attempt must be considered to study the modification on the heater wall because of nanoparticle deposition during boiling phenomenon of nanofluid.

In the current article, the model proposed by Li et al. [32] for $0^\circ \leq \theta \leq 90^\circ$ and $\Delta T_{ONB} \leq \Delta T_{sup} \leq 30\ K$ is employed for nucleation site density calculation by adding the nucleation site density correlation as a user-defined function and validated the current model.

$$N_a\ (\text{sites/cm}^2) = 12,060\ (1 - \cos\theta)\ \Delta T^{2.06}_{sup} \tag{29}$$

Contact angle

The contact angle (θ) is an important property that affects the performance of pool boiling heat transfer as it describes the hydrophilic or hydrophobic

wettability nature. The contact angle depends upon the nanoparticles deposited, nanoparticle concentration, deposition thickness, material of the heater surface, and the thermo-physical properties of working fluid. The contact angle is a combined phenomenon of fluid as well as heater surface. As per the previously published experimental and numerical studies, a static contact angle of 22° ± 2°, 14°± 4°, and 79° were obtained for pool boiling of alumina nanofluid, silica nanofluid, and pure water, respectively, depending upon the concentration of nanofluid [20, 27, 39]. The volume concentration of nanofluid greatly affects the contact angle and with increase in nanofluid concentration, liquid contact angle increases. Therefore, a static contact angle of 23°, 16°, and 79° are considered for the SiO_2/water nanofluid (0.05 vol%), Al_2O_3/water nanofluid (0.05 vol%), and pure water respectively [40] in the present study to obtain the active nucleation site density.

Bubble departure diameter

In the previous findings, most of the empirical correlations were found to depend on bubble contact angle, thermo-hydraulic properties, and wall superheat [41]. The bubble departure diameter is significant bubble dynamics parameters of pool boiling that requires additional research to predict the boiling phenomenon. Cole and Rohsenow [42] proposed a correlation for bubble departure diameter of saturated pool boiling

$$D_d = 1.5e-4\left[\frac{\sigma}{g(\rho_f-\rho_v)}\right]^{0.5}\left(\frac{\rho_f.C_{p,f}.T_{sat}}{\rho_v.h_{fg}}\right)^{1.25} \tag{30}$$

Alimoradi and Shams [43] used following correlation for high-pressure water boiling.

$$D_d = \min\left[0.6\ \exp\left(\frac{-T_{sat}}{45}\right), 1.4\right] \tag{31}$$

In the current article, a polynomial correlation [35] is considered for bubble departure diameter calculation. This correlation is acquired from the experimental outcomes of the study by Gerardi et al. [38]. The given correlation can only be used for the range of following parameters; $\Delta T_{ONB} \le \Delta T_{sup} \le 30\ K$ and $10 \le q'' \le 1500\ \text{kW/m}^2$

$$D_d = -(1.91\times10^{-3}) + (4.211\times10^{-4}\Delta T_{sup}) - \left(1.709\times10^{-5}\ \Delta T_{sup}^2\right) + \left(2.039\times10^{-7}\ \Delta T_{sup}^3\right) \tag{32}$$

Bubble departure frequency and bubble waiting time

Based on the fundamental studies, when consecutive bubbles depart the boiling surface, it merges, and the CHF is achieved. The bubble departure frequency signifies the rate at which bubble departs the heater wall. An increase in bubble departure diameter results a decrease in bubble departure frequency [44]

$$f_b = \frac{1}{D_d^n} \tag{33}$$

where n is index which has a different value. Li et al. [32] used the index as 0.5 and gave the most popular correlation.

$$f_b = \left[\frac{4g(\rho_f-\rho_g)}{3\rho_f D_d}\right]^{0.5} \tag{34}$$

The time lapse between bubble departure and formation of the new bubble in the identical nucleation site is referred as waiting time. Zaboli et al. [23] used the following correlation to calculate the bubble waiting time.

$$t_{bw} = \frac{0.8}{f_b} \tag{35}$$

A coefficient (C_{wt}) is established to rectify the bubble waiting time.

$$C_{wt} = 0.1 + 2.5\ \times\ \left[1 - e^{-\left(\frac{\Delta T_{sup}}{22.44}\right)^{5.9}}\right] \tag{36}$$

Boundary conditions

The partial differential governing equations stated in governing equation section are put through to the following boundary conditions, refer Figure 3.

- A constant heat flux at the heater surface is considered

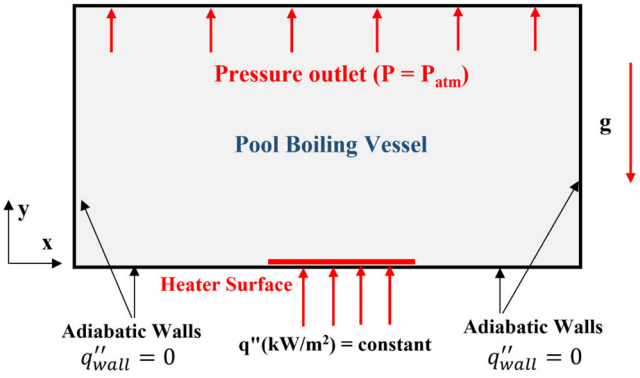

Figure 3. Schematic of computational domain with boundary conditions.

$$q''_w = -k_w \frac{\partial T}{\partial x} = \text{Constant} \quad (37)$$

- The side and bottom walls except heater surface are considered adiabatic having heat flux equal to zero

$$q''_w = -k_w \frac{\partial T}{\partial x} = 0 \quad (38)$$

- No-slip condition at the wall-fluid interface.
- Atmospheric pressure is considered at the upper wall of the boiling vessel

$$P = P_{atm} \quad (39)$$

Thermo-physical properties of nanofluid and heater surface material

The dilute aqueous nanofluids with low concentration (less than 0.1 vol%) are supposed to be favorable coolants for safety systems in nuclear reactors because of their capability for improving the CHF with negligible change in thermo-physical properties from those of base fluid. In this article, the pool boiling of SiO_2/water and Al_2O_3/water having volume concentration of 0.01%, 0.02%, 0.05%, and 0.06% was studied to observe the bubble dynamic behavior. The thermal–physical properties of water, vapor (bubble), nanoparticle, nanofluid, heater surface material can be seen in Table 2 [6, 32, 45]. The bulk property change for nanofluids can be neglected due to the lower volume fraction of nanofluid. A surface tension of 0.0589 N/m at saturation temperature of 100 °C was considered for the water (base fluid). In addition, negligible change in surface tension of nanofluid, i.e. same surface tension for nanofluid and base fluid is considered because of the dilute nanofluid (concentration of nanoparticles less than 0.1 vol%). The following correlation is used to obtain the thermal–physical properties of SiO_2/water and Al_2O_3/water nanofluids at different concentration [46]

$$\rho_{nf} = \varphi.\rho_p + (1 - \varphi)\rho_{bf} \quad (40)$$

$$C_{p,nf} = \frac{\varphi.\rho_p C_{p,p} + (1-\varphi)\rho_{bf} C_{p,bf}}{\varphi\rho_p + (1-\varphi)\rho_{bf}} \quad (41)$$

$$\frac{k_{nf}}{k_{bf}} = \frac{2k_{bf} + k_p - 2\varphi(k_{bf} - k_p)}{2k_{bf} + k_p + \varphi(k_{bf} - k_p)} \quad (42)$$

$$\frac{\mu_{nf}}{\mu_{bf}} = (1-\varphi)^{2.3} \quad \text{for} \quad \varphi \le 2.0\ \% \quad (43)$$

Table 2. Properties of nanofluid at saturation temperature of 100 °C [6, 32, 45].

Working fluid	k (W/m K)	ρ (kg/m^3)	C_p (J/kg K)	μ (kg/m s)
Heater surface material (at 27 °C)				
Cu	400	8,920	385	–
Al	200	2,711	900	–
Brass	109	8,612	395	–
S.S.	15	8,057	480	–
Nanoparticle (at 27 °C)				
SiO_2	1.4	2,220	745	–
Al_2O_3	40	3,880	773	–
Base fluid and vapor (bubble) (at 100 °C)				
Water	0.67909	958.35	4,215	0.000281
Vapor	0.02509	0.59817	2,080	0.000012
SiO_2/water nanofluid (at 100 °C)				
$\varphi = 0.01$ vol%	0.68622	970.96	4,136	0.000274
$\varphi = 0.02$ vol%	0.69343	983.58	4,059	0.000268
$\varphi = 0.05$ vol%	0.71554	1021.43	3,838	0.000249
$\varphi = 0.06$ vol%	0.72306	1034.04	3,768	0.000243
Al_2O_3/water nanofluid (at 100 °C)				
$\varphi = 0.01$ vol%	0.69864	987.56	4,080.44	0.000274
$\varphi = 0.02$ vol%	0.71858	1,016.78	3,952.95	0.000268
$\varphi = 0.05$ vol%	0.78075	1,104.47	3,611.06	0.000252
$\varphi = 0.06$ vol%	0.80231	1,133.68	3,508.82	0.000246

Mesh generation and grid independency

Grid generation is a significant requirement of any computational domain modeling. Therefore, to achieve the pool boiling heat transfer outcomes with maximum accuracy for validation, mess generation and grid sensitivity test are to be carried out. In the finite volume method, the geometrical model is discretized into small elements followed by use of conservation equations to the cells to obtain the discrete equations. The generated mesh consisted of triangular and rectangular cell. Figure 4a shows the mesh generation of computational domain. A fine mesh size was considered for the heater wall. At a fixed heat flux of 300 kW/m^2, the total mess size increased with reduced mess size of heater surface. A grid sensitivity test has been done to obtain the optimum mess size of computational domain. The variation in HTC with total mesh size for grid sensitivity test can be seen in Figure 4b. The variation in pool boiling HTC appeared to be very less after the mesh size of 25,456, which signify toward the correctness of the results. Therefore, total mess size of 25,456 is selected for further simulation. The grid sensitivity test can also be seen from Table 3.

Results and validation

In the present study, the pool boiling of SiO_2/water and Al_2O_3/water nanofluid having volume concentration of $0.01 - 0.06\%$ under saturated boiling and atmospheric pressure condition are studied numerically. The effect of heater surface material and nanofluid concentration on heat transfer performance is studied. A constant heat flux ranging from 100 to 600 kW/m^2 are applied to the heater wall surface. The bubble departure diameter, active nucleation site density, bubble departure frequency, and bubble waiting time are obtained from empirical correlations.

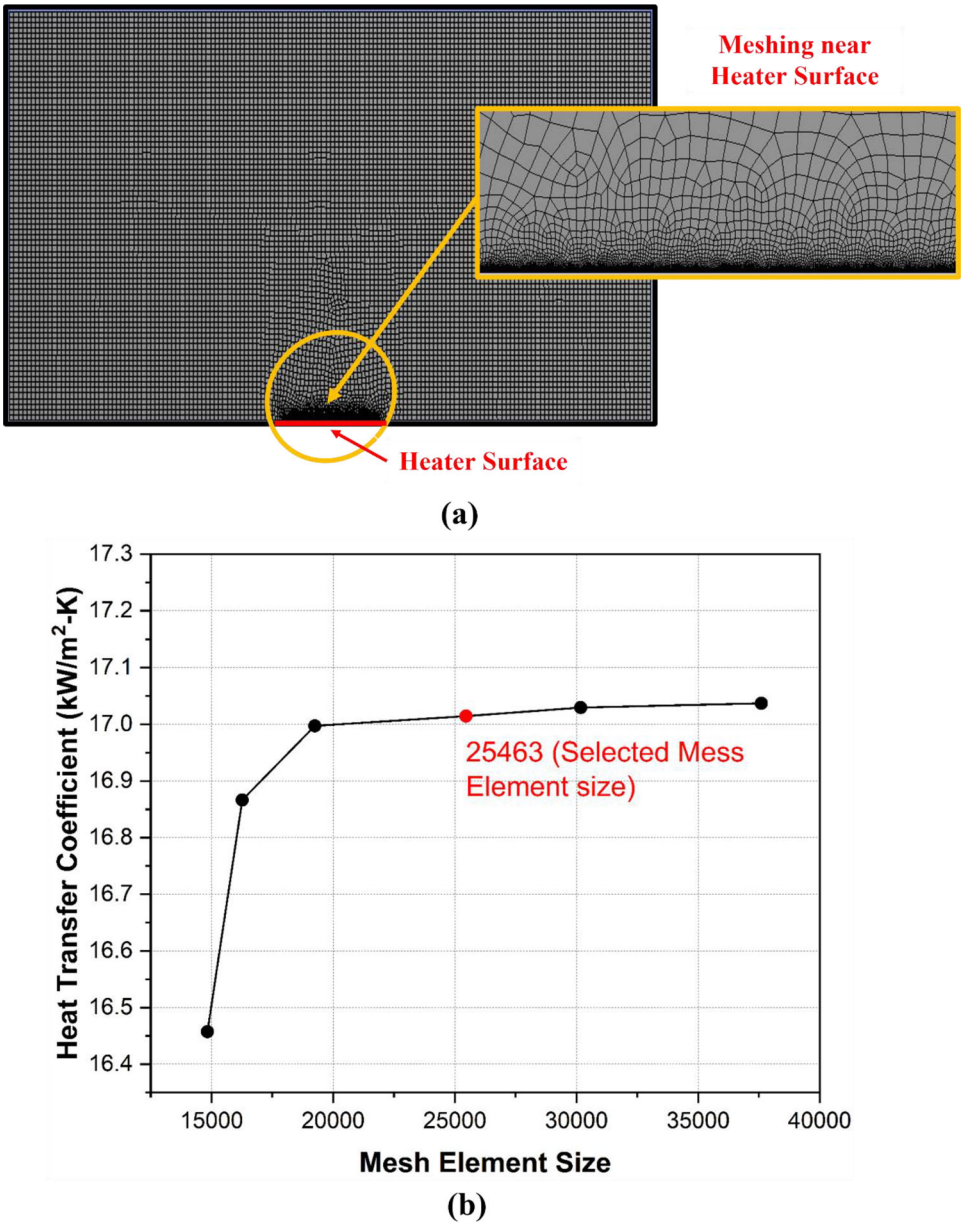

Figure 4. (a) Mesh generation of computational domain and (b) Mesh sensitivity test.

Table 3. Grid sensitivity test.

Heat Flux (kW/m^2)	Total no. of elements	Heater element size (mm)	Heat transfer coefficient (kW/m^2 K)
300	14,910	0.08	16.2451
	16,305	0.07	16.6545
	19,325	0.06	16.9860
	25,530	0.05	17.0114
	30,210	0.04	17.0472
	37,660	0.03	17.1253

Model validation with numerical and experimental results

The present model is validated with numerical studies of Wang et al. [17], Kamel et al. [20], experimental results of Nukiyama [47], and well-known correlation of Rohsenow [48], as shown in Eq. (44). The validation of the present numerical results with previous experimental and numerical results can be seen in Figure 5. Rohsenow [48] performed the pool boiling of de-ionized water using an electrically heated platinum (Pt) wire and gave a most popular correlation

$$\frac{C_{p,\mathrm{f}}\Delta T_{\mathrm{sup}}}{h_{\mathrm{fg}}} = C_{\mathrm{wf}}\left(\frac{q''}{\mu_{\mathrm{f}}h_{\mathrm{fg}}}\sqrt{\frac{q''\sigma_{\mathrm{f}}}{g(\rho_{\mathrm{f}}-\rho_{\mathrm{v}})}}\right)^{0.33}\left(\frac{C_{p,\mathrm{f}}\mu_{\mathrm{f}}}{k_{\mathrm{f}}}\right)^{1.7} \tag{44}$$

The coefficient C_{wf} [Eq. (44)] depends on the type of heater surface–fluid properties combination. The C_{wf} values of 0.017 for the copper plate/water combinations were taken from Pioro et al. [49] for validating the present numerical work. There has been a

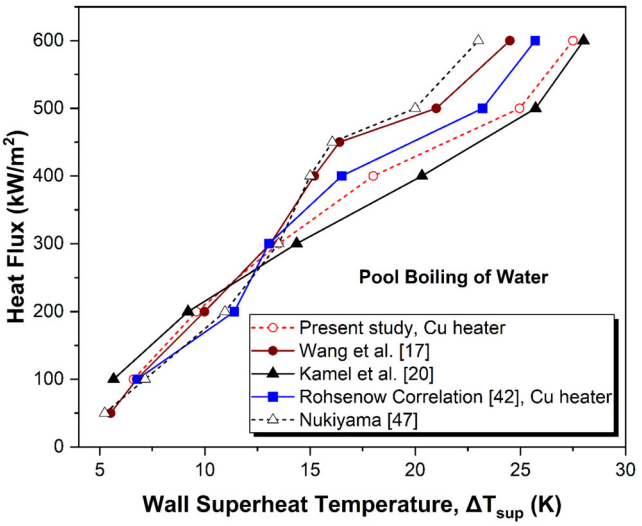

Figure 5. Validation of present results.

marginal deviation in the present findings and the results obtained from Rohsenow [48] correlation. Kamel et al. [20] considered bubble waiting time coefficient (C_{wt}) as unity. But in the present study, for quenching heat flux correction model [shown in Eq. (28)], C_{wt} is obtained by incorporating the empirical correlation [shown in Eq. (36)] as a user-defined function in the boiling parameter list which resulted in the marginal deviation past the superheat wall temperature of 15 K.

The heater surface material effect

The effect of boiling surface (heater) material on wall superheat and HTC are studied for saturated pool boiling of water. The copper, aluminum, brass, and stainless-steel as a heater material are considered. The variation in superheat temperature with heat flux for different boiling surface material can be seen in Figure 6a. At a constant heat flux, reduced wall superheat temperature results in enhancement in pool boiling heat transfer performance. A reduction in wall superheat is advantageous for heat transfer performance enhancement. Since, the saturation temperature of water is constant (100 °C), therefore lower wall superheat will result in lower temperature of heater wall.

A minimum wall superheat (maximum heat transfer performance) was obtained with Cu heater surface and least with stainless steel. A maximum reduction in wall superheat of 21.4%, 14.23%, and 11.03% for Cu, brass and Al heater surface respectively are obtained as compared to that of stainless-steel. The pool boiling of water with brass as a heater surface

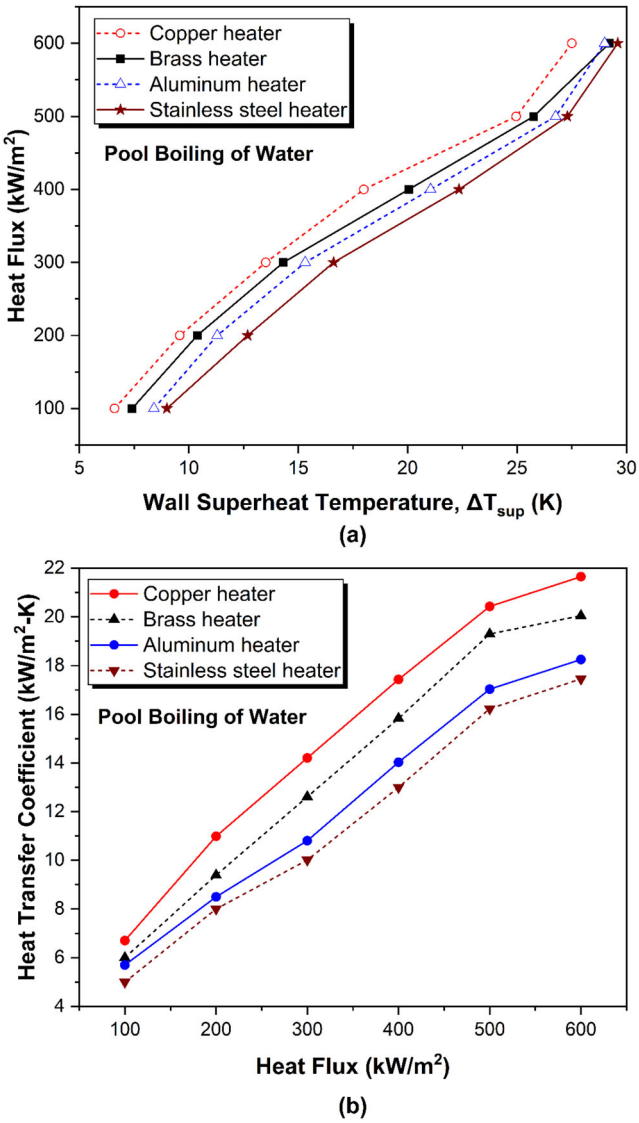

Figure 6. Variation in (a) wall superheat temperature and (b) heat transfer coefficient with heat flux for different heater surface material.

showed enhanced thermal performance than that with aluminum heater surface, even though the thermal conductivity of brass (115 W/m K) is less than that of aluminum (205 W/m K). This concludes that the boiling surface depends on various parameters such as wettability, porosity, specific heat, density apart from thermal conductivity. An abrupt change in slope was noticed after wall superheat of 25 K and heat flux of 500 kW/m^2.

The variation in HTC for different heater wall material can be seen in Figure 6b. The pool boiling of water with Cu heater surface showed maximum HTC whereas stainless steel showed minimum. A maximum enhancement in HTC of 19.14%, 15.27%, and 10.14% for Cu, brass, and Al heater surface respectively are

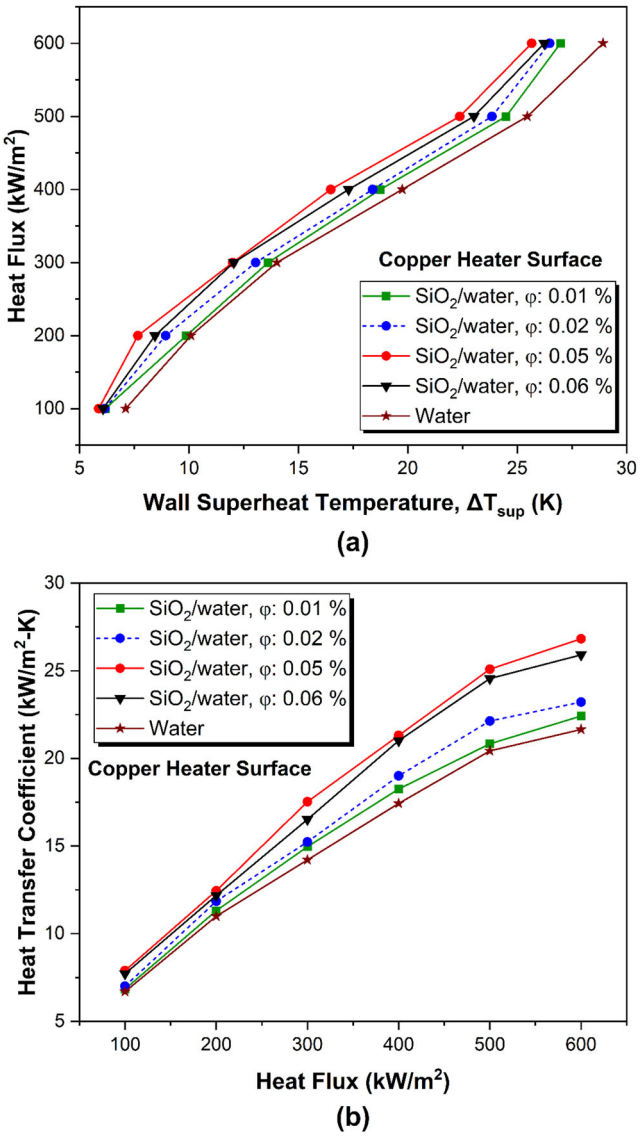

Figure 7. Effect of nanofluid concentration on (a) wall superheat temperature and (b) heat transfer coefficient.

obtained as compared to that of stainless steel. An abrupt decrease in HTC was noticed due to the low rate of bubble formation.

The heat flux effect

The variation in HTC and wall superheat temperature with heat flux can be seen in Figure 6. The HTC increased with increase in heat flux supplied to the heater wall. The nucleation sites density and bubble formation rate enhanced with increase in heat flux. On the other hand, the bubble waiting time reduced with increase in heat flux. The vapor bubbles forms, grows on the heater wall, and then transverse to the working fluid due to the buoyant force effect. The propagation of the bubbles creates a disturbance on the existing interface of liquid–vapor. With increase in heat flux, the thermal momentum shifted from heated wall to the working fluid caused extra disturbance and turbulence inside the working fluid which resulted in faster detachment of bubble along with rapid increase in the liquid velocity near the heater wall. At high heat flux, the void fraction nearby the heater wall is more effective than other location of heater surface. The vapor volume fraction enhanced with rise in heat flux due to the increased bubble formation on the heater wall.

The nanofluid concentration effect

The nanoparticle's material, size, and concentration are the most significant parameter of the nanofluid, as active nucleation site density depends on the deposited nanoparticles on the heater wall during pool boiling of nanofluid. Now considering Cu as a heater surface, the pool boiling of SiO_2/water nanofluid at different concentration are studied. The simulation was performed considering volume concentration of 0.01–0.06% and heat flux in between 100 and 600 kW/m^2. The effect of volume concentration of nanofluid on superheat temperature can be seen in Figure 7a and on HTC can be seen in Figure 7b. The silica nanofluid showed better heat transfer performance than base fluid irrespective of concentration. The pool boiling of nanofluids resulted in a modification on heater surface because of nanoparticle deposition on boiling surface. The thermo-physical properties of the modified boiling surface along with bubble parameter such as nucleation site density, bubble departure diameter, bubble release frequency fluctuates with concentration. An increase in concentration (up to some optimum) resulted in a reduction in wall superheat and thus increment in HTC. The nanoparticle deposition on heater surface develops a nano-porous layer on the heater wall which caused an enhancement in wettability, active nucleation sites, bubble formation at faster rate. The formation of porous layer is because of microlayer evaporation process on the heater wall and this effect is mostly superior at high fluxes.

For a constant heat flux, the maximum decrease in wall superheat and maximum increment in HTC was achieved with 0.05 vol% concentration of nanofluid. At heat flux of 500 kW/m^2, wall superheat is reduced by 4.32, 5.84, 11.15, and 9.82% for 0.01, 0.02, 0.05, and 0.06 vol% concentration respectively as compared to base fluid. A maximum reduction in superheat temperature of 11.15% is obtained with 0.5 vol% of

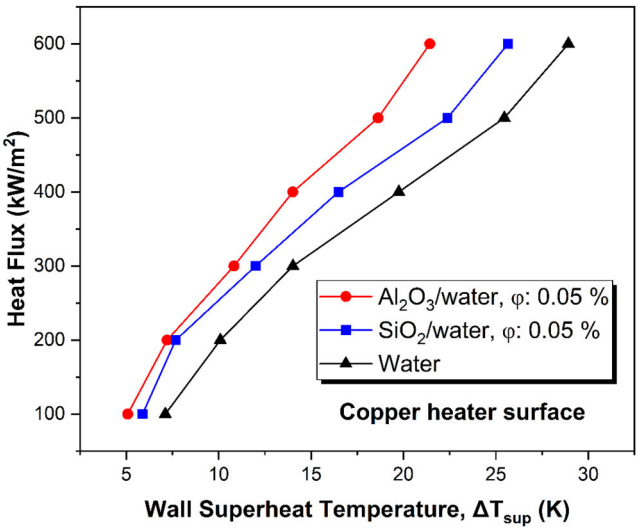

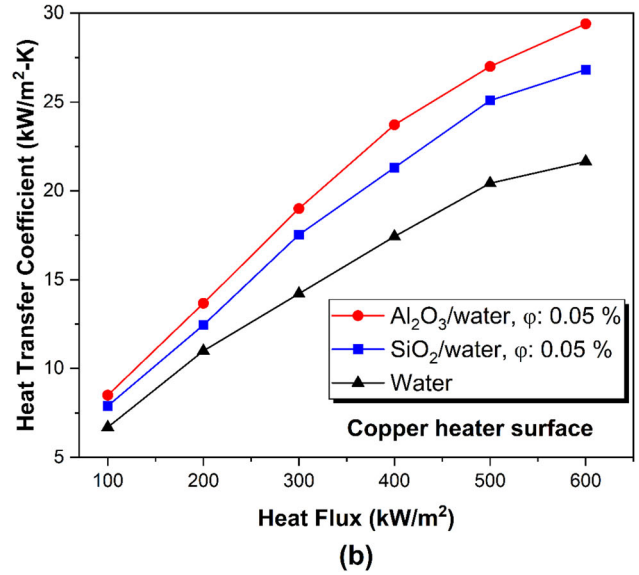

Figure 8. Effect of SiO_2/water and Al_2O_3/water nanofluid at optimum concentration on (a) wall superheat temperature and (b) heat transfer coefficient.

concentration. The HTC enhanced by 2.51, 5.53, 21.85, and 17.71% for 0.01, 0.02, 0.05, and 0.06 vol% concentration respectively at heat flux of 400 kW/m^2 when compared with base fluid.

Types of nanoparticles effect

Al_2O_3/water nanofluid are being used more often in research and industry for cooling purpose, due to their better thermo-physical properties, better wettability, and cost effective. Figure 8 shows the comparison in heat transfer performance of SiO_2/water and Al_2O_3/water nanofluid. The Alumina nanofluid showed better heat transfer coefficient (Figure 8a) and

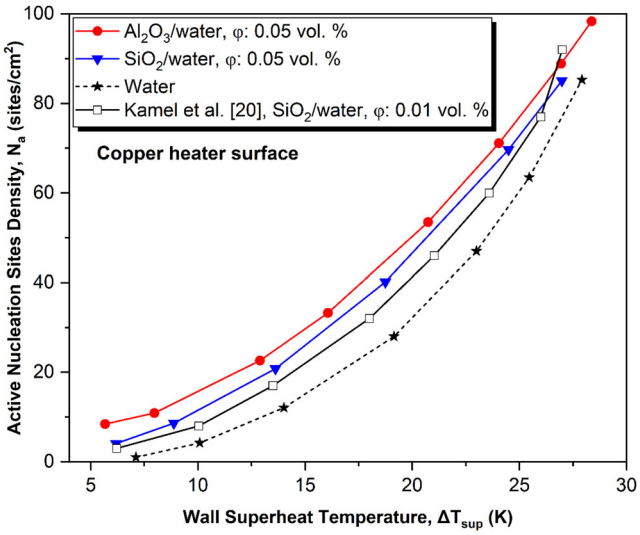

Figure 9. Variation in active nucleation site density with wall superheat temperature.

reduced wall superheat temperature (Figure 8b) as compared to silica nanofluid and base fluid. At optimum concentration of 0.5 vol%, a maximum reduction in wall superheat of 19.25% and 11.15% and maximum enhancement in HTC of 27.74% and 21.85% are obtained for Al_2O_3/water and SiO_2/water nanofluid respectively as compared to the base fluid.

Active nucleation sites density effect

As per the earlier studies, the nucleation sites density, bubble departure diameter, and bubble departure frequency are significant boiling parameter while modeling the pool boiling phenomenon. The active nucleation sites density is obtained by incorporating the empirical correlation [shown in Eq. (29)] as a user-defined function. A static contact angle of 23°, 16°, and 79° are considered for the SiO_2/water nanofluid (0.05 vol%), Al_2O_3/water nanofluid (0.05 vol%), and pure water respectively [20, 27, 39, 40] in the present study to obtain the active nucleation site density. Figure 9 shows the variation in nucleation sites density with superheat temperature. Nucleation sites density enhanced with increase in wall superheat. At a constant volume concentration of nanofluid, the maximum active nucleation sites density on copper heater surface is obtained with alumina nanofluid as compared to silica nanofluid and base fluid. As the concentration of nanofluid increases, contact angle increases which results in an increment in nucleation site density. This enhancement in nucleation site density caused a reduction in bubble departure diameter which leads to separation of bubbles from the

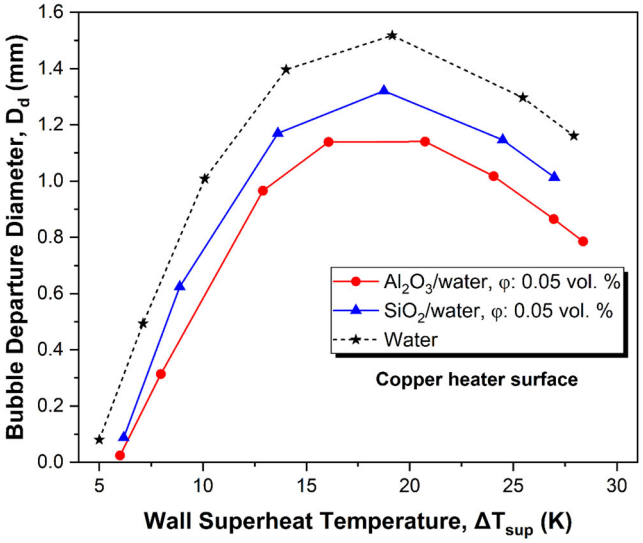

Figure 10. Variation in bubble departure diameter with wall superheat temperature.

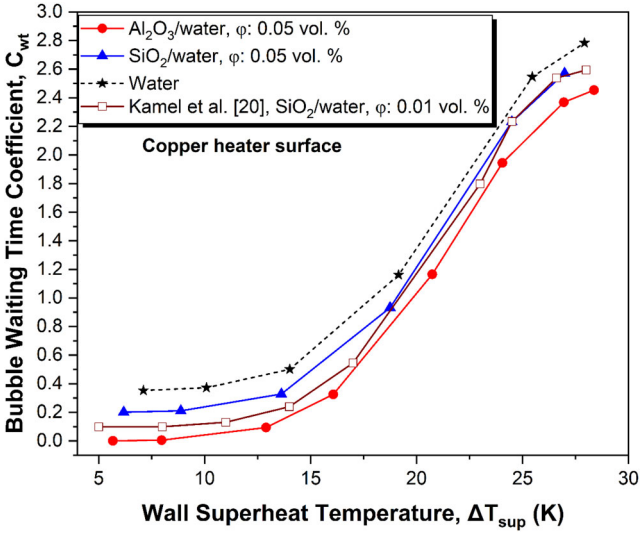

Figure 11. Variation in bubble waiting time coefficient with wall superheat temperature.

boiling surface at a faster rate (also called as bubble release frequency), which finally decreases the superheat temperature and increases the HTC. The current model is compared with the results of Kamel et al. [20] in which they performed pool boiling of silica nanofluid considering nanofluid concentration of 0.01 vol%. In the present study, an optimum concentration of 0.05 vol% has been obtained and entire analysis have been done considering 0.05 vol% due to which a marginal deviation in the active nucleation site density below wall superheat temperature of 25 K has been observed.

Bubble departure diameter effects

As per the previous studies, the bubble departure diameter is the function of wall superheat, boiling surface, and working fluid. In present study, the bubble departure diameter is obtained by incorporating the correlation [shown in Eq. (32)] as a user-defined function. The variation in bubble departure diameter with superheat temperature is shown in Figure 10. With increase in superheat temperature, an increase in departure diameter up to an optimum value is observed and then it reduces as wall superheat continues to rise. At a particular wall superheat temperature, the minimum departure diameter has been obtained for alumina nanofluid and maximum for water. A reduction in bubble departure diameter results in increase in the bubble departure frequency, which is the favorable aspect in the pool boiling phenomenon. As the departure diameter decreases, a faster rate of detachment of bubbles from the heating area is observed, leading to a reduction in wall superheat temperature and an enhancement in HTC. As the bubbles depart from the heater wall, its size reduces and the development in merging of bubble reduces, which results in delay of CHF. As the heat flux rises, nucleated bubbles from the heater wall results in bubble coalescence which further reduces the bubbles formation.

Bubble waiting time effect

The time lapse between the bubble departure and formation of the new bubble in identical nucleation site is referred as waiting time. The bubble waiting time coefficient is established to rectify the waiting time for bubble departure. The bubble waiting time coefficient is obtained by incorporating the empirical correlation [shown in Eq. (36)] as a user-defined function. Figure 11 shows the variation in bubble waiting time coefficient with superheat temperature. An increment in bubble waiting time coefficient with increase in wall superheat is observed. An insignificant variation in C_{wt} below wall superheat of 12 K is noticed. At a particular wall superheat temperature, minimum bubble waiting time coefficient is obtained for Al_2O_3/water nanofluid and maximum for water. With rise in bubble waiting time, the bubble detachment frequency from the heater wall slows down and the bubbles leave the heater surface with larger diameter. Therefore, a minimum bubble waiting time for enhanced bubble release frequency and reduced bubble departure diameter is the favorable aspect in the pool boiling phenomenon.

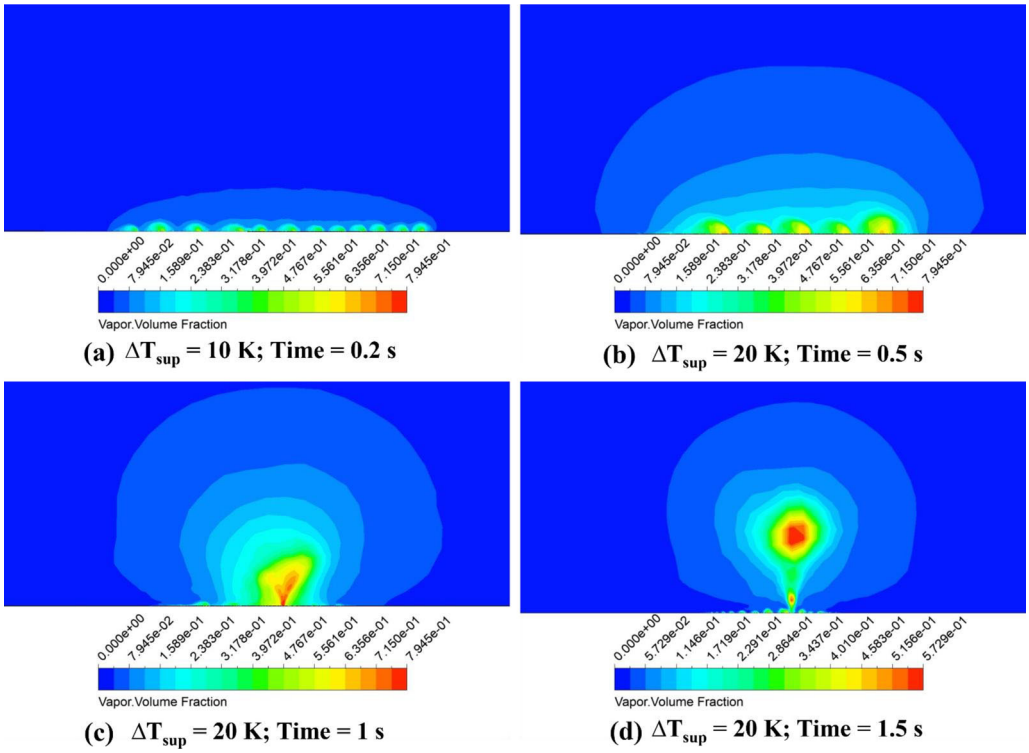

Figure 12. Formation and growth of vapor volume fraction for SiO_2/water nanofluid (0.05 vol%) at constant wall superheat temperature of 20 K over time of (a) $t = 0.2$ s, (b) $t = 0.5$ s, (c) $t = 1$ s, and (d) $t = 1.5$ s.

Distribution of vapor volume fraction

The vapor bubbles forms, grows at the heater wall, and then transverse to the nanofluid. The propagation of the bubbles creates a disturbance on the existing interface of liquid–vapor. For the hydrophilic characteristics of heater wall, the nucleation sites density and bubble formation rate enhanced with increase in heat flux. On the other hand, the bubble waiting time reduces with increase in heat flux. The contours of the formation and growth of vapor volume fraction on a heater surface during pool boiling of nanofluid under transient simulation can be seen from Figure 12. At $t = 0.2$ s, the bubble generation phenomenon commences and proceeds in time, an increment in the vapor volume fractions is observed. The bubbles begin to propagate in vertical direction inside the pool boiling chamber and wakes begins to form at the lower portion of the bubble. The bubbles continues to grow with time and detaches from the wakes. At $t = 1$ s, bubble begins to collapse as it propagates away from the boiling surface due to the fluid resistance. At $t = 1.5$ s, new bubbles start to form on the heater wall. In present case, the cycle period of the bubble leaving the heater surface is more.

The variation in vapor volume fraction of Al_2O_3/water nanofluid (0.05 vol%) with different superheat temperature at specific time of $t = 1.5$ s can be seen in Figure 13. An enhancement in vapor volume fraction with increase in wall superheat is observed. As the boiling surface temperature increases during NPB of nanofluid, the evolution of bubble from the cavities increases which results in enhancement in nucleation site density and increases the formation of bubble at faster rate. Due to buoyancy force, the bubble transverses in vertical direction. A lower void fraction for nanofluid is noticed as related to that of water due to the inter-phase interaction of nanoparticle with vapor bubbles. The void fraction nearby the heater wall is more effective than other location due to the high heat flux at the heater wall. The deposition of nanoparticle during pool boiling of nanofluid caused an increased capillary wicking force which enhanced the nucleation sites density by occupying the microcavities on heater wall and resulting in enhancement in wettability. Therefore, a lower void fraction than water in this domain is observed.

The comparison in vapor volume fraction of water, silica, and alumina nanofluid (0.05 vol%) at specific time of $t = 1.5$ s and superheat temperature of 20 K can be seen in Figure 14. The pool boiling of alumina nanofluid showed maximum vapor volume fraction as compared to silica nanofluid and water. The vapor

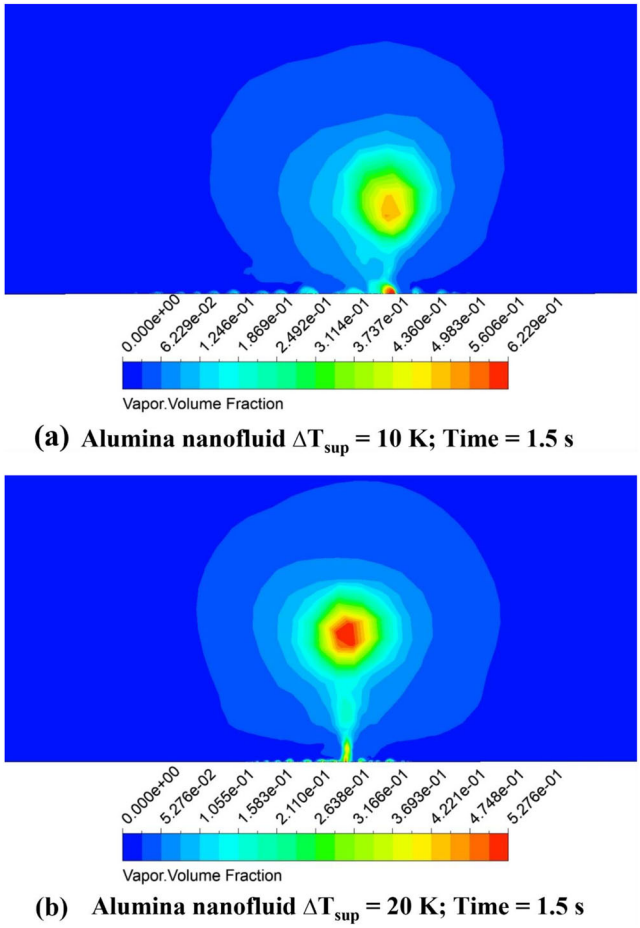

Figure 13. Vapor volume fraction of pool boiling of Al_2O_3/water nanofluid (0.05 vol%) at $t = 1.5$ s and wall superheat temperature of (a) $\Delta T_{sup} = 10$ K and (b) $\Delta T_{sup} = 20$ K.

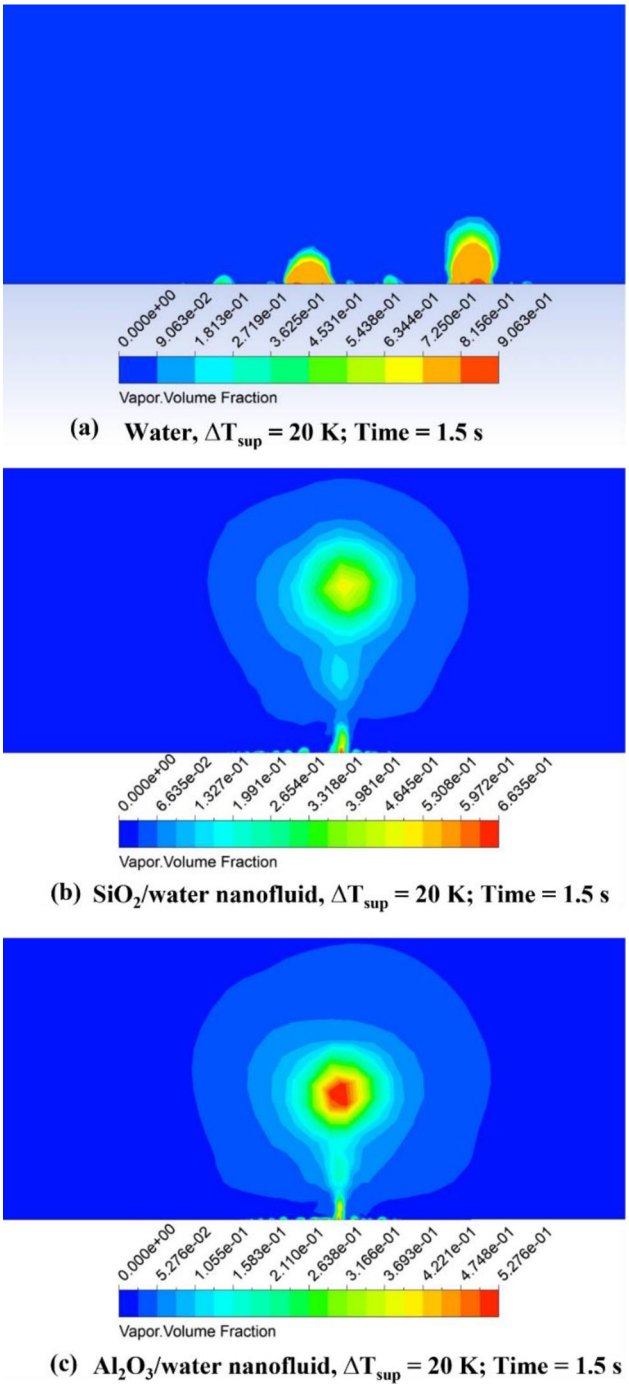

Figure 14. Variation in vapor volume fraction at wall superheat temperature of 20 K and $t = 1.5$ s for (a) water, (b) SiO_2/water nanofluid (0.05 vol%), and (c) Al_2O_3/water nanofluid (0.05 vol%).

velocity during the pool boiling of nanofluid is an essential concern because of dependency of condenser performance in the multi-phase condensation mechanism. Therefore, the vapor velocity prediction might help the pool boiling study.

The streamlines over a time for silica nanofluid (0.05 vol%) at superheat temperature of 20 K can be seen from Figure 15. The bubble velocity is initiated from the center of heater wall and there is no bubble evolution at the corners to prevent the movement of bubble on side walls. An increment in bubble velocity with increase in wall superheat is observed because of increased bubble formation from the active nucleation sites on the heater wall. At wall superheat of 20 K, the bubbles merges and propagates from the heater wall's center, which makes it considerable with a velocity lower than upper bubbles due to the resistance of liquid around. The velocity of nanofluid advancing toward the adiabatic walls decreases and attains its minimum value while it increases near the heater surface. This decrease in velocity near adiabatic wall is mainly due to the reduction in thermal momentum and increase in velocity near heater wall due to enhancement in thermal momentum which results in additional agitation. During commencement of bubble generation on heater wall, the agitation process results in the formation of eddies on heater surface. These vorticities that assisted the movement of water to the

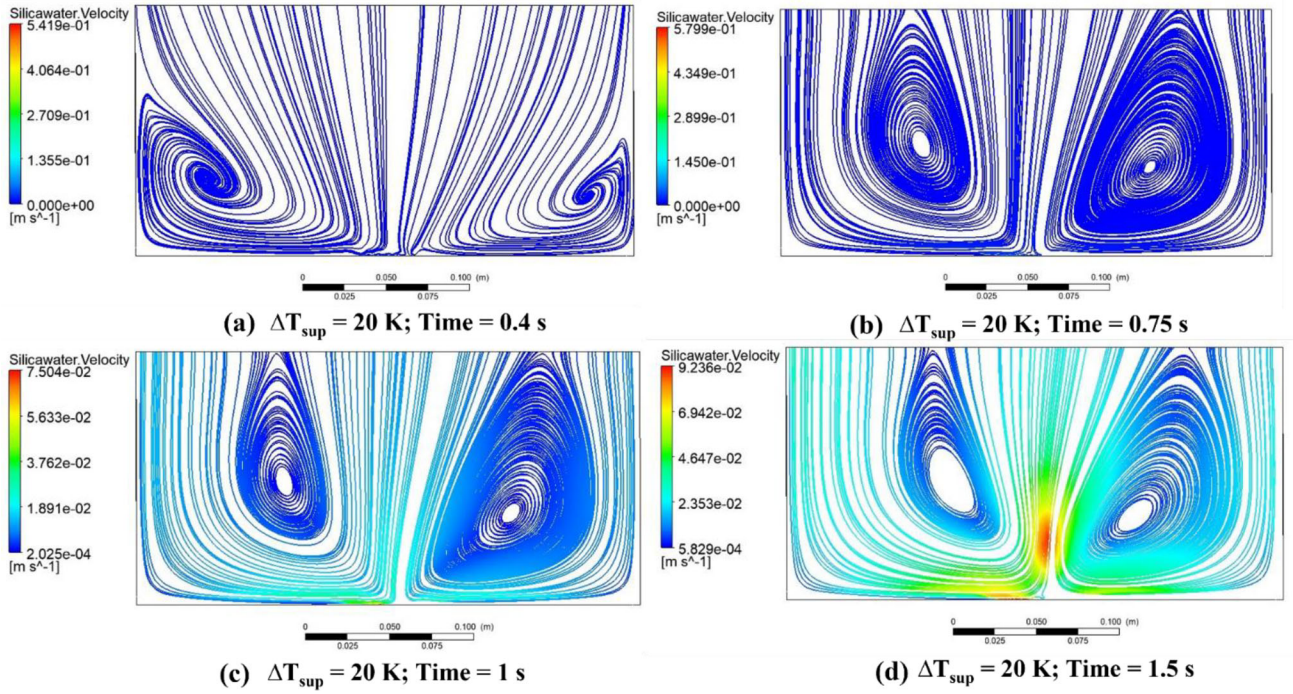

Figure 15. Evolution of streamlines for silica nanofluid at wall superheat temperature of 20 K over time (a) $t = 0.4$ s, (b) $t = 0.75$ s, (c) $t = 1$ s, and (d) $t = 1$.

heater wall still have existence over a period under the vapor fraction and their effect as the bubble size enhances, this effect increases as the bubble diameter grows. With rise in heat flux, the vapor volume fraction enhances due to the bubble generation on the heater wall. The vapor bubbles seemed to be vigorous on hearer surface and propagates in vertical direction due to the buoyant force effect.

Conclusions

The method of involving bubble evolving process, bubble dynamics phenomenon, and distribution of vapor void fraction altogether while modeling and simulation of pool boiling of nanofluid have been the motivation behind present research work. The current study is of great importance and will contribute to the reduction in energy consumption in various heat transfer devices and better heat transfer performance of thermal systems for various practical applications such as recovery and reuse of the wastewater and incinerator heat, cooling of high heat flux generating micro-electronics chips, cooling of fast breeder test reactor in which reactor core is placed inside the coolant, etc.

In present study, the NPB of Al_2O_3/water and SiO_2/water nanofluid under saturated temperature and atmospheric pressure condition are studied numerically. A constant heat flux ranging from 100 to 600 kW/m^2 and nanofluid concentration of 0.01 to 0.06 vol% are considered. The two-phase Eulerian approach, heat flux wall-partitioning, and RPI boiling model are considered to simulate the current model. The deposition of nanoparticle on heater surface using pool boiling of nanofluid resulted in generation of small nanoporous cavities, increased active nucleation sites density, and bubble release frequency which further enhanced the HTC and reduced wall superheat. The main conclusions are as follows:

- A maximum reduction in wall superheat of 21.4%, 14.23%, and 11.03% and maximum enhancement in HTC of 19.14%, 15.27%, and 10.14% are obtained for Cu, brass, and Al heater surface respectively as compared to stainless-steel. The pool boiling heat transfer with brass (k: 115 W/m K) as a heater surface showed enhanced thermal performance than that with Al (k: 205 W/m K), which concludes that the boiling surface parameter not only depends thermal conductivity, but also on wettability, porosity, specific heat, density, etc.
- A maximum reduction in superheat temperature and maximum increment in HTC was achieved

with 0.5 vol% concentration of nanofluid. At a constant heat flux of 500 kW/m^2, wall superheat is reduced by 4.32%, 5.84%, 11.15%, and 9.82% and HTC enhanced by 2.51%, 5.53%, 21.85%, and 17.71% for 0.01, 0.02, 0.05, and 0.06 vol% concentration respectively as compared to base fluid.

- Al_2O_3/water nanofluid showed better heat transfer performance than SiO_2/water nanofluid. At optimum concentration of 0.5 vol%, the maximum reduction in wall superheat of 19.25% and 11.15% and the maximum enhancement in HTC of 27.74% and 21.85% are obtained for Al_2O_3/water and SiO_2/water nanofluid respectively as compared to the base fluid.
- The pool boiling of nanofluids resulted in the formation of small cavities on heater surface due to nanoparticle deposition which enhanced the porosity, wettability, nucleation site density, bubble departure frequency. The formation of nanoporous layer is because of microlayer evaporation process on the heater wall.
- Nucleation sites density enhanced with increase in wall superheat. As the concentration of nanofluid increases, contact angle increases which resulted in an increment in nucleation site density. This enhancement in nucleation site density caused a reduction in bubble departure diameter which leads to separation of bubbles from the boiling surface at a faster rate, which finally reduced the wall superheat and increased the HTC.
- The bubble departure diameter increased up to a certain level with increase in superheat temperature and then it reduced as wall superheat continues to increase. A maximum increase in bubble departure diameter of 1.3 mm was observed at superheat temperature of 20 K.
- Bubble departure frequency enhanced with decrease in bubble departure diameter, which is favorable aspect in pool boiling phenomenon.
- The bubble waiting time coefficient has been established to rectify the waiting time for bubble departure. An increment in bubble waiting time coefficient with increase in wall superheat is observed. An insignificant variation in bubble waiting time coefficient was noticed below wall superheat of 12 K.

Funding

This Research was supported by the Science and Engineering Research Board (SERB), India under Grant No. CRG/2021/001457.

Notes on contributors



Sudhir Kumar Singh is a Ph.D. research scholar in the Mechanical Engineering Department at National Institute of Technology Hamirpur, H.P., India. He graduated in Mechanical Engineering from RTU Kota, Rajasthan, India in 2011 and M. Tech in Thermal Engineering from Thapar University Patiala, India in 2018. He is currently working on pool boiling heat transfer enhancement using surface modifications.



Deepak Sharma is an Assistant Professor in the Department of Mechanical Engineering at National Institute of Technology Hamirpur, H.P., India since 2018. He received Ph.D. degree in Mechanical Engineering from National Institute of Technology, Silchar, Assam, India in 2018, M. Tech degree from the same institute in the year of 2013 and bachelor's degree from GLA University, Mathura, U.P in the year of 2010. His research interests include, boiling heat transfer, renewable energy, heat exchangers, and thermal hydraulics in nuclear reactors.



Akshay Kumar Singh is a M. Tech research scholar in the Mechanical Engineering Department at National Institute of Technology Hamirpur, H.P., India. He graduated in Mechanical Engineering from Dr. APJ Abdul Kalam Technical University, U.P., India in 2016. His research interests include numerical simulations and pool boiling heat transfer.

References

[1] S. Mukherjee, S. Ebrahim, P. C. Mishra, N. Ali, and P. Chaudhuri, "A review on pool and flow boiling enhancement using nanofluids: nuclear reactor application," *Processes*, vol. 10, no. 1, pp. 177, Jan. 2022. DOI: 10.3390/pr10010177.

[2] M. M. Mahmoud and T. G. Karayiannis, "Pool boiling review. I. Fundamentals of boiling and relation to surface design," *Therm. Sci. Eng. Prog.*, vol. 25, pp. 101024, Oct. 2021. DOI: 10.1016/j.tsep.2021.101024.

[3] A. Marie, S. Cioulachtjian, S. Lips, and V. Sartre, "Thermal interactions between nucleation sites and the solid wall during pool boiling of a pure fluid: A review," *Int. J. Therm. Sci.*, vol. 174, pp. 107388, Apr. 2022. DOI: 10.1016/j.ijthermalsci.2021.107388.

[4] M. Khooshehchin, A. Mohammadidoust, and S. Fathi, "Experimental investigation of stabilizers of nanofluid in the pool boiling process," *Heat Transf.*

Eng., vol. 44, no. 5, pp. 442–460, 2023. DOI: 10.1080/01457632.2022.2068220.

[5] A. Ranjan, I. Ahmad, R. K. Gouda, M. Pathak, and M. K. Khan, "Enhancement of critical heat flux (CHF) in pool boiling with anodized copper surfaces," *Int. J. Therm. Sci.*, vol. 172, no. part B, pp. 107338, Feb. 2022. DOI: 10.1016/j.ijthermalsci.2021.107338.

[6] H. Aminfar, M. Mohammadpourfard, and M. Sahraro, "Numerical simulation of nucleate pool boiling on the horizontal surface for nano-fluid using wall heat flux partitioning method," *Comput. Fluids*, vol. 66, pp. 29–38, Aug. 2012. DOI: 10.1016/j.compfluid.2012.05.019.

[7] H. Yeom, K. Sridharan, and M. L. Corradini, "Bubble dynamics in pool boiling on nanoparticle-coated surfaces," *Heat Transf. Eng.*, vol. 36, no. 12, pp. 1013–1027, 2015. DOI: 10.1080/01457632.2015.979116.

[8] I. S. Kiyomura, L. L. Manetti, A. P. da Cunha, G. Ribatski, and E. M. Cardoso, "An analysis of the effects of nanoparticles deposition on characteristics of the heating surface and ON pool boiling of water," *Int. J. Heat Mass Transf.*, vol. 106, pp. 666–674, Mar. 2017. DOI: 10.1016/j.ijheatmasstransfer.2016.09.051.

[9] A. Nazari and S. Saedodin, "Porous anodic alumina coating for optimisation of pool-boiling performance," *Surf. Eng.*, vol. 33, no. 10, pp. 753–759, 2017. DOI: 10.1080/02670844.2016.1199187.

[10] G. Song, P. A. Davies, J. Wen, G. Xu, and Y. Quan, "Nucleate pool boiling heat transfer of SES36 fluid on nanoporous surfaces obtained by electrophoretic deposition of Al_2O_3," *Appl. Therm. Eng.*, vol. 141, pp. 143–152, Aug. 2018. DOI: 10.1016/j.applthermaleng.2017.12.068.

[11] X. Quan, D. Wang, and P. Cheng, "An experimental investigation on wettability effects of nanoparticles in pool boiling of a nanofluid," *Int. J. Heat Mass Transf.*, vol. 108, pp. 32–40, May 2017. DOI: 10.1016/j.ijheatmasstransfer.2016.11.098.

[12] H. Noh *et al.*, "Effect of surface structure and coating on the heat transfer deflection behavior in the early stage of nucleate boiling," *Int. J. Heat Mass Transf.*, vol. 126, no. part A, pp. 1315–1322, Nov. 2018. DOI: 10.1016/j.ijheatmasstransfer.2018.05.122.

[13] M. Ray and S. Bhaumik, "Nucleate pool boiling heat transfer of hydro-fluorocarbon refrigerant R134a on TiO_2 nanoparticle coated copper heating surfaces," *Heat Transf. Eng.*, vol. 40, no. 12, pp. 997–1006, 2019. DOI: 10.1080/01457632.2018.1450333.

[14] S. M. A. Noori Rahim Abadi, A. Ahmadpour, and J. P. Meyer, "Numerical simulation of pool boiling on smooth, vertically aligned tandem tubes," *Int. J. Therm. Sci.*, vol. 132, pp. 628–644, Oct. 2018. DOI: 10.1016/j.ijthermalsci.2018.07.005.

[15] N. Gobinath, T. Venugopal, K. Palani, and A. A. Samuel, "Numerical modelling of thermophoresis in water-alumina nanofluid under pool boiling conditions," *Int. J. Therm. Sci.*, vol. 129, pp. 1–13, Jul. 2018. DOI: 10.1016/j.ijthermalsci.2018.02.025.

[16] R. R. Gupta, S. Bhambi, and V. K. Agarwal, "CFD modeling for nucleate pool boiling of nanofluids," *Numeric. Heat Transf. Part A Appl.*, vol. 75, no. 6, pp. 402–412, 2019. DOI: 10.1080/10407782.2019.1591863.

[17] J. Wang, M. Diao, and X. Liu, "Numerical simulation of pool boiling with special heated surfaces," *Int. J. Heat Mass Transf.*, vol. 130, pp. 460–468, Mar. 2019. DOI: 10.1016/j.ijheatmasstransfer.2018.10.120.

[18] F. Pourfattah *et al.*, "Numerical simulation of the effect of using nanofluid in phase change process of cooling fluid," *Int. J. Numeric. Methods Heat Fluid Flow*, vol. 30, no. 6, pp. 2913–2934, Jan. 2020. DOI: 10.1108/HFF-12-2018-0806.

[19] A. Akbari, S. A. Alavi Fazel, S. Maghsoodi, and A. S. Kootenaei, "Pool boiling heat transfer characteristics of graphene-based aqueous nanofluids," *J. Therm. Anal. Calorim.*, vol. 135, no. 1, pp. 697–711, Jan. 2019. DOI: 10.1007/s10973-018-7182-2.

[20] M. S. Kamel, M. S. Al-Agha, F. Lezsovits, and O. Mahian, "Simulation of pool boiling of nanofluids by using Eulerian multiphase model," *J. Therm. Anal. Calorim.*, vol. 142, no. 1, pp. 493–505, Oct. 2020. DOI: 10.1007/s10973-019-09180-x.

[21] E. Çiftçi and A. Sözen, "Heat transfer enhancement in pool boiling and condensation using h-BN/DCM and SiO/DCM nanofluids: Experimental and numerical comparison," *Int. J. Numeric. Methods Heat Fluid Flow*, vol. 31, no. 1, pp. 26–52, Jan. 2021. DOI: 10.1108/HFF-02-2020-0113.

[22] S. K. Singh and D. Sharma, "Review of pool and flow boiling heat transfer enhancement through surface modification," *Int. J. Heat Mass Transf.*, vol. 181, pp. 122020, Dec. 2021. DOI: 10.1016/j.ijheatmasstransfer.2021.122020.

[23] S. Zaboli, H. Alimoradi, and M. Shams, "Numerical investigation on improvement in pool boiling heat transfer characteristics using different nanofluid concentrations," *J. Therm. Anal. Calorim.*, vol. 147, no. 19, pp. 10659–10676, Mar. 2022. DOI: 10.1007/s10973-022-11272-0.

[24] A. R. Harikrishnan, P. Dhar, P. K. Agnihotri, S. Gedupudi, and S. K. Das, "Effects of interplay of nanoparticles, surfactants and base fluid on the surface tension of nanocolloids," *Eur. Phys. J. E Soft Matter*, vol. 40, no. 5, pp. 53, 2017. DOI: 10.1140/epje/i2017-11541-5.

[25] A. R. Harikrishnan, P. Dhar, P. K. Agnihotri, S. Gedupudi, and S. K. Das, "Wettability of complex fluids and surfactant capped nanoparticle-induced quasi-universal wetting behavior," *J. Phys. Chem. B*, vol. 121, no. 24, pp. 6081–6095, Jun. 2017. DOI: 10.1021/acs.jpcb.7b02723.

[26] A. R. Harikrishnan, P. Dhar, S. Gedupudi, and S. K. Das, "Governing Influence of Thermodynamic and Chemical Equilibria on the Interfacial Properties in Complex Fluids," *J. Phys. Chem. B*, vol. 122, no. 14, pp. 4141–4148, Apr. 2018. DOI: 10.1021/acs.jpcb.7b12008.

[27] X. Li, K. Li, J. Tu, and J. Buongiorno, "On two-fluid modeling of nucleate boiling of dilute nanofluids,"

Int. J. Heat Mass Transf., vol. 69, pp. 443–450, Feb. 2014. DOI: 10.1016/j.ijheatmasstransfer.2013.10.037.

[28] P. I. Shyamkumar, S. Singh, A. Srivastava, and M. Visaria, "Numerical investigation of nucleate pool boiling heat transfer for different superheat conditions," *Heat Transf. Eng.*, vol. 43, no. 1, pp. 83–100, 2022. DOI: 10.1080/01457632.2020.1844450.

[29] S. C. P. Cheung, S. Vahaji, G. H. Yeoh, and J. Y. Tu, "Modeling subcooled flow boiling in vertical channels at low pressures. I. Assessment of empirical correlations," *Int. J. Heat Mass Transf.*, vol. 75, pp. 736–753, Aug. 2014. DOI: 10.1016/j.ijheatmasstransfer.2014.03.016.

[30] H. Salehi and F. Hormozi, "Numerical study of silica-water based nanofluid nucleate pool boiling by two-phase Eulerian scheme," *Heat Mass Transf.*, vol. 54, no. 3, pp. 773–784, Mar. 2018. DOI: 10.1007/s00231-017-2146-9.

[31] M. Ishii and N. Zuber, "Drag coefficient and relative velocity in bubbly, droplet or particulate flows," *AIChE J.*, vol. 25, no. 5, pp. 843–855, Sep. 1979. DOI: 10.1002/aic.690250513.

[32] X. Li, Y. Yuan, and J. Tu, "A parametric study of the heat flux partitioning model for nucleate boiling of nanofluids," *Int. J. Therm. Sci.*, vol. 98, pp. 42–50, Dec. 2015. DOI: 10.1016/j.ijthermalsci.2015.06.020.

[33] M. Ishii, "Two-fluid model for two-phase flow,"*Multiphase Sci. Technol.*, vol. 5, no. 1–4, pp. 1–63, 1990. DOI: 10.1615/MultScienTechn.v5.i1-4.10.

[34] M. Lopez de Bertodano, R. T. Lahey, and O. C. Jones, "Turbulent bubbly two-phase flow data in a triangular duct," *Nucl. Eng. Des.*, vol. 146, no. 1-3, pp. 43–52, Feb. 1994. DOI: 10.1016/0029-5493(94)90319-0.

[35] H. Alimoradi, S. Zaboli, and M. Shams, "Numerical simulation of surface vibration effects on improvement of pool boiling heat transfer characteristics of nanofluid," *Korean J. Chem. Eng.*, vol. 39, no. 1, pp. 69–85, Jan. 2022. DOI: 10.1007/s11814-021-0895-0.

[36] W. E. Ranz, "Evaporation from drops, Parts I & II," *Chem. Eng. Prog.*, vol. 48, pp. 141–146, 1952.

[37] N. Kurul and M. Z. Podowski, "Multidimensional effects in forced convection subcooled boiling," presented at the Proceedings of the 9th International Heat Transfer Conference, Jerusalem, Israel, vol. 2, pp. 21–26, 1990.

[38] C. Gerardi, J. Buongiorno, L.-W. Hu, and T. McKrell, "Study of bubble growth in water pool boiling through synchronized, infrared thermometry and high-speed video," *Int. J. Heat Mass Transf.*, vol. 53, no. 19-20, pp. 4185–4192, Sep. 2010. DOI: 10.1016/j.ijheatmasstransfer.2010.05.041.

[39] A. Inbaoli, C. S. Sujith Kumar and S. Jayaraj, "A review on techniques to alter the bubble dynamics in pool boiling," *Appl. Therm. Eng.*, vol. 214, pp. 118805, Sept. 2022. DOI: 10.1016/j.applthermaleng.2022.118805.

[40] S. J. Kim, I. C. Bang, J. Buongiorno and L. W. Hu, "Surface wettability change during pool boiling of nanofluids and its effect on critical heat flux," *Int. J. Heat Mass Transf.*, vol. 50, no. 19–20, pp. 4105–4116, Sept. 2007. DOI: 10.1016/j.ijheatmasstransfer.2007.02.002.

[41] D.-S. Guo *et al.*, "Numerical study on the behavior of vapor bubbles during boiling with surface acoustic wave (SAW)," *Int. J. Heat Mass Transf.*, vol. 192, pp. 122928, Aug. 2022. DOI: 10.1016/j.ijheatmasstransfer.2022.122928.

[42] R. Cole and W. M. Rohsenow, "Correlation of bubble departure diameters for boiling of saturated liquids," *Chem. Eng. Prog. Symp. Ser.*, vol. 65, no. 92, pp. 211–213, 1969.

[43] H. Alimoradi and M. Shams, "Optimization of subcooled flow boiling in a vertical pipe by using artificial neural network and multi objective genetic algorithm," *Appl. Therm. Eng.*, vol. 111, pp. 1039–1051, Jan. 2017. DOI: 10.1016/j.applthermaleng.2016.09.114.

[44] K. Mondal and A. Bhattacharya, "Bubble dynamics and enhancement of pool boiling in presence of an idealized porous medium: a numerical study using lattice Boltzmann method," *J. Therm. Sci. Eng. Appl.*, vol. 14, no. 8, pp. 081004, Aug. 2022. DOI: 10.1115/1.4053054.

[45] E. William, A. James, Jr., and S. Chickos, "Thermophysical properties of fluid systems" in *NIST Chemistry WebBook*, P. J. Linstrom and W. G. Mallard, Eds., NIST Standard Reference Database Number 69, National Institute of Standards and Technology, Gaithersburg, MD, USA, 2022.

[46] A. R. I. Ali and B. Salam, "A review on nanofluid: preparation, stability, thermophysical properties, heat transfer characteristics and application," *SN Appl. Sci.*, vol. 2, no. 10, pp. 1636, Oct. 2020. DOI: 10.1007/s42452-020-03427-1.

[47] S. Nukiyama, "The maximum and minimum values of the heat Q transmitted from metal to boiling water under atmospheric pressure," *Int. J. Heat Mass Transf.*, vol. 9, no. 12, pp. 1419–1433, 1966. DOI: 10.1016/0017-9310(66)90138-4.

[48] W. M. Rohsenow, "A method of correlating heat-transfer data for surface boiling of liquids," *Trans. Am. Soc. Mech. Eng.*, vol. 74, no. 6, pp. 969–975, Aug. 1952. DOI: 10.1115/1.4015984.

[49] I. L. Pioro, W. Rohsenow and S. S. Doerffer, "Nucleate pool-boiling heat transfer. II: assessment of prediction methods," *Int. J. Heat Mass Transf.*, vol. 47, no. 23, pp. 5045–5057, Nov. 2004. DOI: 10.1016/j.ijheatmasstransfer.2004.06.020.